Controllable Synthetic Molecular Channels: Biomimetic Ammonia Switch

Alexey V. Titov, Boyang Wang, Kyaw Sint, and Petr Král*

Department of Chemistry, University of Illinois at Chicago, Chicago, Illinois 60607

Received: October 30, 2009; Revised Manuscript Received: November 25, 2009

We use molecular dynamics simulations combined with iterative screening to test if one can design mechanically controllable and selective molecular pores. The first model pore is formed by two stacked carbon nanocones connected by aliphatic chains at their open tips, in analogy to aquaporins. It turns out that when one nanocone is gradually rotated with respect to the other, the molecular chains alter the size of the nanopore formed at the cone tips and control the flow rates of liquid pentane through it. The second model pore is formed by two carbon nanotubes joined by a cylindrical structure of antiparallel peptides. By application of a torque to one of the nanotubes, while holding the other, we can reversibly fold the peptides into forward or backward-twisted barrels. We have modified the internal residues in these barrels to make these pores selective and controllable. Eventually, we found a nanopore that in the two folded configurations has very different transmission rates for hydrated NH_3 molecules.

Introduction

Biological ionic and molecular channels play a key role in cellular transport phenomena.[1] Most of them are protein channels with cores formed by precisely arranged arrays of amino acids that efficiently recognize and guide the passing species.[2] Their selectivity is achieved by intriguing concerted dynamics of the molecular passage through channels with complex Coulombic and van der Waals (vdW) potentials.[3] For example, β-barrel channels[4] are formed by antiparallel hydrogen-bonded β sheets helically wrapped into cylinders. Other channels can have different symmetries or forms, such as the tetrameric aquaporins[5−7] and tetrameric ion channels.[8,9] The profile of some biological channels can be modulated in response to voltage gating,[10] ligand binding,[11] or mechanical deformation.[12]

Artificial protein channels could be designed de novo[13−15] or assembled from legolike pieces[16] and fine-tuned by a "directed evolution".[17] Biomimetic constructions of molecular channels can rely on more synthetic approaches.[18,19] For example, synthetic channels can be made from ring peptides, coupled by hydrogen bonds,[20,21] or Coulombically.[22] These systems might be incorporated and activated inside biological membranes.[23,24] Ionic and molecular channels could also be made of inorganic materials, such as zeolites,[25] carbon,[26] silica,[27] and other materials.[28,29] The inorganic channels are often not selective or transparent enough for various refined applications. Therefore, nanochannels with novel structures and recognition principles need to be designed.

Molecular dynamics (MD) simulations have predicted[30] and experiments have demonstrated fast transport of gases[31,32] and liquids[33−35] through carbon nanotube (CNT) membranes. Hydrated ions could pass through CNTs of large enough diameters[36] and drag molecules on CNT surfaces.[37,38] Nanocones[39] with open tips or graphene sheets with nanopores[40] could also form nanofluidic channels. Although, the selectivity of these inorganic channels is rather limited,[41,42] their passage rates might be controlled mechanically[43,44] and electronically.[45]

These optimistic results show that synthetic functional channels can, in principle, be designed. But there are many open problems associated with this possibility. Here, we want to explore some of these limitations on model systems that reveal what qualities one might expect in such systems and what obstacles we might need to overcome. In our test studies, we combine the properties of biological and synthetic nanopores to design model hybrid nanochannels, formed by covalently connected carbon nanocones or nanotubes with aliphatic or peptide chains.[46] The selectivity of these nanochannels is tuned by mutations of the peptide residues and their transport rates are controlled by their mechanical deformations.[47]

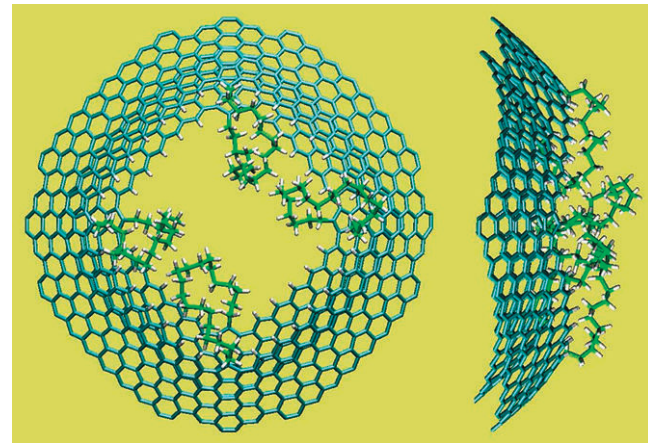


Figure 1. The stacked (untwisted) pair of nanocones connected with four -$(CH_2)_{13}$- alkyl chains around the central pore. (left) Bottom view form the tip. (right) The side view.

Results and Discussion

Molecular Nanovalve. First, we design a model molecular valve formed by two stacked carbon nanocones with the C_4 symmetry,[39] as shown in Figure 1. The cone tips have a total disclination angle of TD = 120° (apex angle 84.6°).[48] The inner and outer cones are formed by three and four layers of benzene rings, respectively, and have square open tips with the sizes of 15 × 15 Å^2 and 20 × 20 Å^2. In principle, one could open the cone tips by oxidation reactions[49,50] and realize their bonding

* To whom correspondence should be addressed: E-mail: pkral@uic.edu.

10.1021/jp9103933 © 2010 American Chemical Society
Published on Web 12/11/2009

with the chains by aromatic substitution reactions.[51,52] Four alkyl -$(CH_2)_{13}$- chains are covalently attached to the cones at the corners of their square-shaped tips. In the absence of external forces, these relatively long chains are loosely folded between the two cone tips so that a nanopore is formed at the center.

This hybrid system is reminiscent of tetrameric channel proteins, such as aquaporins.[5−7] The $\pi-\pi$ stacking of the cones allows precise and reproducible rotation of one cone with respect to the other. If we mutually rotate them by a certain angle θ_{rot}, the chains become stretched, helically wrapped, and entangled inside the nanopore. Therefore, we should be able to change the nanopore size by changing θ_{rot} and control the flow of fluids through it.

The MD simulations of the molecular flows through the synthetic nanochannels described here are performed with the NAMD package.[53] We estimate parameters of atoms in aliphatic groups, various molecules, CNTs, and nanocones from similar atom types and add them to the CHARMM27 force field.[54] The time step is always 2 fs, and the Langevin dynamics is always applied with the damping coefficient 0.01 ps^{-1} to minimize the unphysical loss of momenta to the reservoirs.[37,38]

In our MD simulations, we solvate the nanocones with alkyl chains in liquid pentane and study its passage through the nanopore under pressure, when the cones are rotated by the angle θ_{rot}. At each rotation configuration, the pressure of $P = 5-140$ atm is applied to the pentane molecules, and each simulation runs for $t = 100-500$ ns. We count the number of pentanes passing through the pore N_p within the simulation time t and calculate the average flow rate $R = N_p/t$.

We simulate the alkane-cone nanovalves in the NVT ensemble. The stacked cones are placed in a periodic box of 47 × 47 × 37 $Å^3$ filled with pentane. The cones are aligned along the z axis and located at -15 Å $< z < 0$. A layer of fixed dummy atoms is used to cover the plane of the simulation cell around the cones and block the fluid flow around the pore. Initially, the four corners of the outer cone are fixed, and a torque of $\tau = 4.8$ nN nm is applied to the inner cone to induce their mutual rotation. After the inner cone is rotated by the angles of $\theta_{rot} =$ 0, 30, and 60°, the four corners of the inner cone are also fixed. At each θ_{rot}, the pressure of $P = 5-140$ atm is applied to the pentane molecules, by applying forces to the carbon atoms in all the pentanes in the region of $5 < z < 10$ Å. The number of pentanes passing through the nanopore, N_p, is calculated by counting the number of molecules passing through a 7 × 7 $Å^2$ square cross section area located at the nanopore center. In this way, we avoid counting largely fluctuating molecular passages through other regions of the system.

In Figure 2, we plot the dependence of the flow rates R on the pressure P at $\theta_{rot} = 0$, 30, and 60°. It turns out that R depends dramatically on both parameters. At $\theta_{rot} = 0°$, the cone is practically open and R is nonzero even at small pressures. At large pressures, R grows and is practically proportional to the pressure. At $\theta_{rot} = 30°$, the flow is almost zero at low pressures ($P < 10$ atm), since the cone is largely closed. At higher pressures, the cross section area of the nanopore becomes bigger,[55] and the trend is similar as at $\theta_{rot} = 0°$, but R is almost constant in the region of $P = 10-40$ atm. At $\theta_{rot} = 60°$, the flow is practically zero up to $P = 40$ atm, where the four alkyl chains start to give up the high pressure. Then, the system gains the usual dependence, although with smaller flows.

In the inset of Figure 2, we also show the time dependence of the total number of pentanes that pass the nanopore at $P =$ 20 atm. The size of the time-dependent fluctuations in N_p reflect fluctuations in the sizes of the nanopore, caused by the alkyl chains that rotate and change their conformations. For more

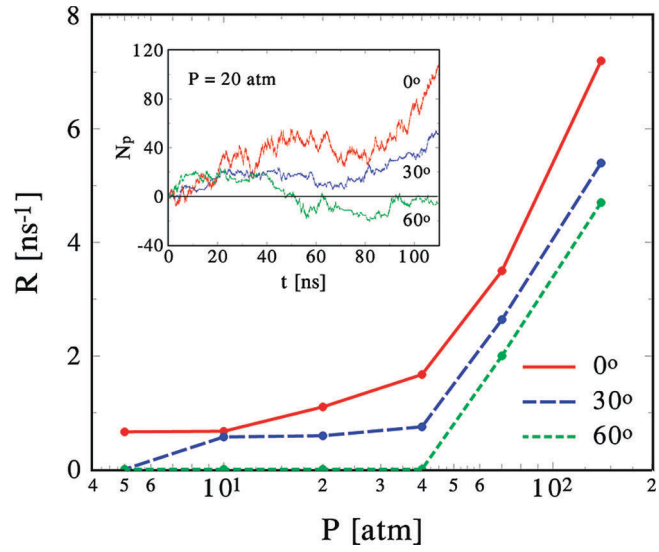


Figure 2. Dependence of the rate of pentane flow through the nanopore on the applied pressures, at rotation angles of $\theta_{rot} = 0$, 30, and 60°. (inset) The time dependence of total number of pentane molecules that pass the nanopore N_p at the applied pressure of $P = 20$ atm and different θ_{rot}.

closed pores, the fluctuations of N_p are smaller, due to stretched alkyl chains. We could further modify these twistable nanopores in order to make them selective to the passing molecules. One possibility is to functionalize the blocking chains. Alternatively, we can avoid connecting the cones by chains and rather attach various functional groups to the cone tips. These functionalized nanocones can be stacked to form longer nanochannels that in their interior might resemble protein channels.

Biomimetic Ammonia Switch. In the following, we implement biological components to address the *selectivity* issue in our search of controllable synthetic molecular channels. We examine model hybrid nanochannels formed by short peptides stretched between two narrow carbon nanotubes, as shown in Figure 3. The peptide structures could be twisted and folded into a barrel,[4] by applying a torque to one of the nanotubes, which thus plays a role of a "chaperon".[56] Once the channels are mutated in their interior, they could potentially have different passage rates in their two (oppositely) folded forms. Because of the large number of possible mutations, we optimally modify the systems[57] and screen them for selective molecular flows.

The hybrid nanochannels, shown in Figure 3, are formed by 5 pairs of antiparallel peptide strands that are "one-to-one" matched and covalently bonded to the terminal C atoms in two (20,0) CNTs. The C and N termini of the peptide form ester and amide bonds, respectively, with every second carbon (in total 10) at each CNT end. The remaining terminal carbons in the CNTs are replaced by nitrogens, forming embedded quinoline-like structures, which have low vdW coupling to the peptides. The peptide strands used are composed of the Asp, Gly, and aLys amino acids. Here, aLys denotes the (L)-2,3-diamino propanoic acid (C_α-CH_2-NH_2 side chain), which has in its side chain three carbons less than lysine.

The "parallel" system, shown in a twisted form in the top part of Figure 3, is formed by 5 pairs of antiparallel peptides, each having the structure -aLys-Gly-aLys-Gly- and -Asp-Gly-Asp-Gly-. In each pair, one peptide is positively charged, with ~0.8 e on each aLys residue, while the other (parallel) peptide is negatively charged, with ~−0.8 e on each Asp residue. The "chessboard" system, shown in the bottom part of Figure 3, is formed by 5 pairs of peptides, each having the structure -aLys-Gly-Asp-Gly- and -Asp-Gly-aLys-Gly-. The charged residues

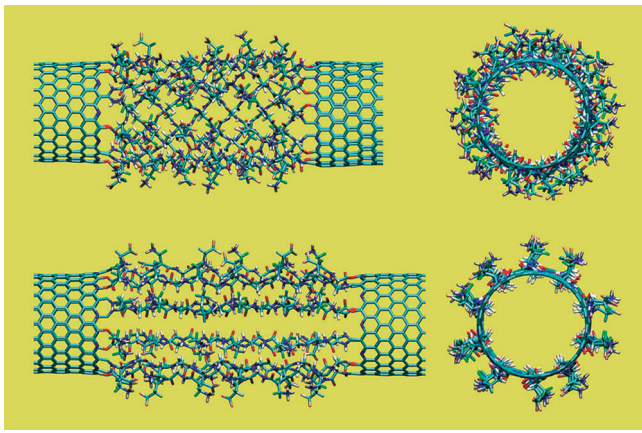


Figure 3. Two types of 12-residue hybrid nanochannels solvated in water at $T = 300$ K. (top) The "parallel" structure folds into a helical form under the external torque of $\tau \approx 14$ nN nm. (bottom) The "chessboard" structure remains straight and ordered for $\tau < 0.7$ nN nm.

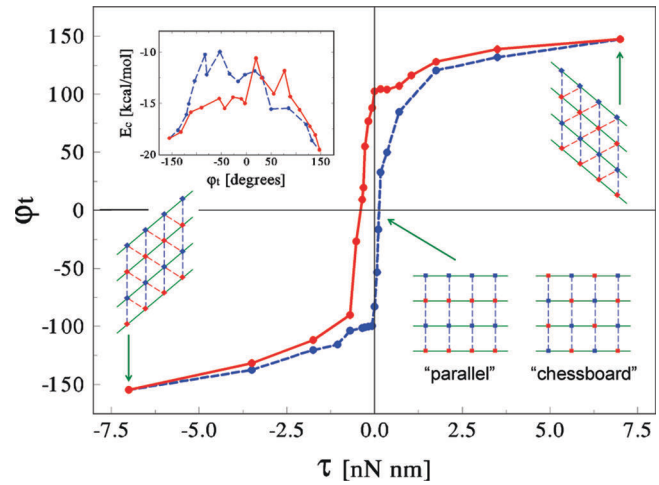


Figure 4. The twist angle-torque hysteresis curve obtained in one cycle for the parallel 8-residue structure. Additional schemes show the charges and their mutual coupling in the straight and twisted structures. (inset) The related Coulombic energy-twist angle hysteresis curve.

in the two systems form a parallel-like and chessboard-like patterns, as shown in the inset of Figure 4.

Reversible Folding of Hollow Nanochannels. We investigate first the (hollow) parallel and chessboard nanochannels, formed by peptide strands with 8, 12, and 16 residues and solvated in water. We use MD simulations to investigate their structure, dynamics, and stability, when they are twisted by the applied external torque. During their potential folding under the applied torque, supportive atoms are used to allow rotation and translation of the CNTs around their common axis, and the CNT ends are kept open for the passage of water solvent. We study the folding dynamics and stability of the CNT-peptide-based nanochannel in the NPT ensemble and apply the Langevin Piston method,[58] with the pressure of $P = 1$ atm and $T = 300$ K, in a periodic simulation cell of $38 \times 38 \times 124$ Å^3. During the simulations, one CNT is fixed and the other is rotated by a torque τ and left to move freely only in the axial direction, by an external bearing of additional atoms.[59]

In the absence of torque, both types of structures stay in straight configurations. In the parallel structure, shown in top part of Figure 3, the antiparallel arrangement of the chiral peptides, where positive chains go in one direction and adjacent negative chains go in the other direction, leads to asymmetric Coulombic binding between the neighboring chains and their preferential pairing; this effect is also partly seen in the chessboard structure in the bottom right part of Figure 3. The strong coupling distinguishes this peptide cylinder from the weakly hydrogen-bonded β barrels.[4] As a result of the chain pairing, the relatively long structure with 16-residue peptides has the tendency to form randomly distributed openings of the diameter of 4−7 Å, allowing the passage of small molecules. The 8-residue peptides, with much fewer degrees of freedom, form an almost uniform cylinder. In contrast, the chessboard systems have stronger Coulombic attractions both within and between the peptide chains, leading to structures with practically no openings, as shown in the bottom part of Figure 3.

In the presence of a small torque, $\tau < 1.4$ nN nm, applied to the two CNTs and oriented in either of the two possible directions, the 8- and 12-residue parallel structures fold within $t \approx 2$ ns to twisted but partly disordered forms with "imploded" chains. The water molecules, confined in the interior of the slowly twisting and longitudinally contracting structures, have enough time to diffuse out of their open ends, without providing radial support to the folding chains. When these shorter structures, with fewer degrees of freedom than the 16-residue structures, are folded under larger torques, water does not have enough time to flow out of them and it applies large pressures on the folding chains, so they are less likely to develop defects. For $\tau \approx 14$ nN nm, the folding of the 12-residue structure takes only about $t \approx 60$ ps, and the folded structure is very ordered and smooth, as shown in the top part of Figure 3. All three (8-, 12-, and 16-residue) parallel structures also fold better under larger Langevin damping, which might be practically realized at lower temperatures or more viscous solvents. This effect is known from protein folding in vitro.[60]

The misfolded 8 and 12-residue parallel structures can be healed, if we hold them under the torque of $\tau = 1.4$ nN nm, close their CNT ends, and apply for 1 ns a pressure of $P \approx 200$ and 500 atm to the water in their interior, respectively. This large hydrostatic pressure inflates the structures, in analogy to protein folding from disordered to native states. In contrast to the parallel structure, the chessboard systems show resistance to small torques and remain stable in straight forms. At $\tau > 0.7$ nN nm, they fold too but become significantly disordered.

We study further only the refoldable (controllable) parallel nanochannels. To understand better their stability, we have exposed them to periodic folding and refolding and analyzed the obtained results. In Figure 4, we present the hysteresis curve for the dependence of the twist angle on the torque applied to the parallel 8-residue structure. The results are obtained in one twisting trajectory going between the two end points (wrapped cylinders) and back, where each data point is averaged over 1000 frames separated by 100 fs, after equilibration for 1 ns. The hysteresis curve is not fully symmetric with respect to the coordinate origin, because the constituent peptides are chiral. The nonzero values of the twist angle at zero torque reflect the Coulombic barriers built in the junction during its folding, similar to natural proteins.[60]

The stability of these structures is controlled by their free energy $G = H - TS$. The entropy S, formed by the vibrational and rotational components, should not change much during the twisting,[61] except the backbone rotational entropy that might slightly decrease when the peptide chains get closer to each other. Since $\Delta E_{tot} \approx \Delta H$, we only estimate the total potential energy of the structures. The total energy

$$E_{tot} = E_{tor} + E_c + E_{vdW} + E_b + E_a + E_d \qquad (1)$$

is formed by the torque energy E_{tor}, the Coulombic energy E_c, the van der Waals energy E_{vdW}, the bond stretching energy E_b,

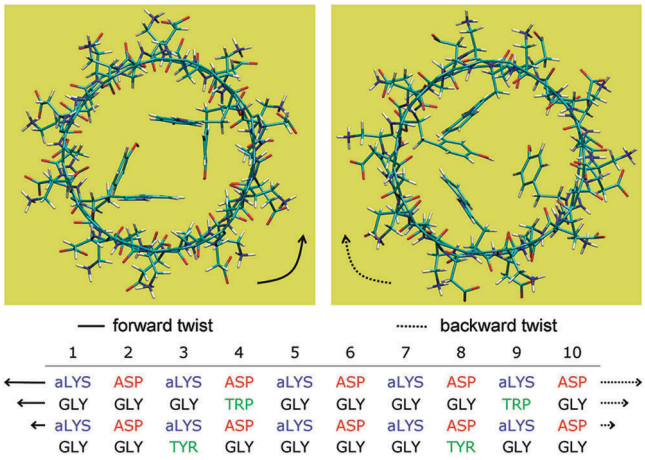


Figure 5. Axial view of the two twisted configurations of the parallel 4-residue 10-peptide junction, with 2 tryptophan and 2 tyrosine residues in its interior. (left) The tryptophan and tyrosine side chains shadow each other, so the channel is relatively open. (right) The interior side chains are spread, so the channel is blocked more. (bottom) Amino acid sequence map of 4-residue 10-peptide junction. Each column corresponds to a peptide chain, and the odd/even rows are residues with side chains that are exposed outward/inward. Arrows on the sides schematically represent the relative angular displacement for each row upon twisting in the two directions.

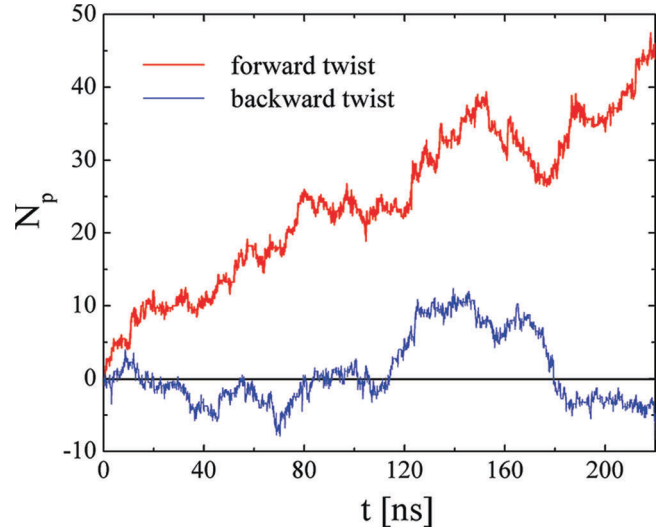


Figure 6. The time dependence of the total number N_p of NH_3 molecules passed through the twisted nanochannels. We can see that practically only the forward twisted channel allows the ammonia molecules to pass.

the angle bending energy E_a, and the dihedral torsional energy E_d. We approximately evaluate these energies by the VMD package[62] for the whole junctions including both CNTs.

During the folding, the E_b and E_a energies are almost constant, E_d gets more positive, signaling the rotation of peptide backbones, while E_{vdW} becomes more negative, because the strands gain more contact points. The increase of E_d seems to largely cancel the decrease of E_{vdW}. Therefore, we focus only on the Coulombic energy

$$E_c = \frac{1}{4\pi\varepsilon_0\varepsilon}\sum_{i<j}\frac{q_i q_j}{r_{ij}} \qquad (2)$$

where q_i are the charges of the atoms, r_{ij} describes the distance between the ith and jth atoms, ε_0 is the vacuum permittivity, and $\varepsilon \approx 80$ is the dielectric constant of water.[63]

In the inset of Figure 4, we display the corresponding variation of the Coulombic energy E_c during the periodic refolding of the structure. It significantly decreases at larger twist angles, because the peptide chains slide on each other and bring closer their oppositely charged residues (schemes in the insets). This explains the stabilization of the parallel systems in the folded forms, reflected by the hysteresis curve in Figure 4. E_c also shows large fluctuations, due to the quasirandom character of electrostatic connectivity between the charged residues. The fluctuations could be smoothed out after averaging over many trajectories (samples), but the hysteresis would not disappear unless the structures are equilibrated for a significantly longer time, allowing thermally assisted exploration of their phase spaces. Folding proteins also show similar hysteresis behavior.[64,65]

Control of Molecular Passage through Mutated Nanochannels. Next, we test if one can modify the above designed nanochannels to make them *selective* and *controllable*. We use short 4-residue peptidesr to increase the stability of the parallel channels during their folding. We start replacing some of the glycines in the hollow interior of the peptide barrel by tryptophans (Trp) and tyrosines (Tyr) that have weakly polar bulky side chains. The mutations are realized at positions where the effective cross section of the channel for the hydrated molecules is largely changed with the twist direction. Each designed channel is tested for the flow of hydrated polar molecules through its interior in the two folded configurations. In a year long simulations on a fast 32 -core computer cluster, we have studied about 15 different channels and passed 5−10 different molecules through them for $t = 100 - 250$ ns.

In Figure 5, we display the most promising system that has very different passage rates for NH_3 molecules in its two oppositely twisted configurations. In the lower part of the figure, we display the detailed amino acid sequence map of the 4-residue peptides. In the forward twist, two pairs of interior residues shadow each other, thus increasing the cross section area available for the NH_3 passage. As seen from the map, these residues are also physically as close as they can be, i.e., practically behind each other (only residues in the second and fourth lines point inward the barrel). In the backward twist, the Trp and Tyr residues are spread around the circumference of the channel, reducing thus the cross section area available for the NH_3 passage. During the simulations of the flow, the side chains of Trp and Tyr residues do not change their spatial orientations very much, due to local steric constraints.

In the simulations, the channel is twisted in the two configurations and placed in a simulation box with periodic boundary conditions. The open CNT ends become adjacent with their periodic images and form a closed periodic pipeline. We place 10 NH_3 molecules inside the nanochannel and fill the rest of its interior with water under normal pressure. Water also fill the simulation box outside the nanochannel. The flow is realized by pressuring waters from one side of the nanochannel with the pressure of $P \approx 10$ atm. The pressure-driven fluid passage is studied in the NVT ensemble with the unit cell of 38 × 38 × 75 Å^3, where the CNT ends have minimal distances (∼3.8 Å) with their periodic images, forming a closed periodic pipeline. The solution is passed through the channel by applying a constant force on oxygen atoms in a narrow region inside one of the nanotubes,[37] which generates a pressure of $P \approx 10$ atm. Smaller pressures lead to longer simulation times, while larger pressures influence the channel structure. The passing molecules are counted in a 7 × 7 Å^2 square area located at the center of the nanochannel.

In Figure 6, we plot the number N_p of NH_3 molecules passed under steady-state conditions through the channel within the

simulation time t. The results show dramatically different flow rates, $R_{NH_3} = N_p/t$, for the forward and backward twisted configurations of the channel, $R^{for}_{NH_3} \approx 0.18$ ns^{-1}, $R^{bac}_{NH_3} \approx 0$, respectively. The configurational selectivity is very likely caused by the strong 3D asymmetry in the trigonal pyramidal geometry of NH_3, which can be discriminated by the complex 3D potential profile in the oppositely twisted configurations. The flow rates of water for the forward and backward-twisted configurations are nearly identical, $R_{wat} \approx 2.1$ ns^{-1}.

In our extensive screening, we have also used longer peptides, redesigned in all the cases the amino acids at different positions inside the nanochannel, and tested the passage rates of other molecules, such as small sugars, methanol, ethanol, propanol, formaldehyde, and CO_2. These molecules either have planar geometry (water and formaldehyde) or approximately cylindrical geometry (methanol, ethanol, and propanol). Although, not all the channels were tested with all the molecules, the presented system was the only one that manifested significant discrimination.

Conclusions

In conclusion, we have tested the possibility of designing selective and controllable nanochannels for the passage of small molecules. It turns out that these properties could be achieved on model systems. In real systems, the mechanical control might be rather hard to practically realize due to synthetic problems. Therefore, other mechanisms of control might be tested that could lead to similar results. The observed molecular selectivity is also rather unique in synthetic channels. It shows that careful molecular tuning might facilitate this level of selectivity in molecules that might be otherwise hard to separate. Although experimental synthetic nanochannels can be based on the described principles, their structures might be very different from the discussed models.[66,67] Such nanochannels could serve in medical and biological applications, such as in selective collection and delivery of molecules and signals inside cells. Potentially, they might also have a variety of industrial applications, such as in molecular separation or purification.

Acknowledgment. The extensive simulations were done at the computer cluster of the Department of Chemistry, UIC, and the NERSC and NCSA networks. B.W. and K.S. would like to acknowledge the support from the Paaren Fellowships.

Supporting Information Available: Video of mechanical twisting of the nanochannel, formed between two CNT rims. This material is available free of charge via the Internet at http://pubs.acs.org.

References and Notes

(1) MacKinnon, R.; Cohen, S. L.; Kuo, A. L.; Lee, A.; Chait, B. T. *Science* **1998**, *280*, 106–109.
(2) Doyle, D. A.; Cabral, J. M.; Pfuetzner, R. A.; Kuo, A. L.; Gulbis, J. M.; Cohen, S. L.; Chait, B. T.; MacKinnon, R. *Science* **1998**, *280*, 69–77.
(3) Gumbart, J.; Wang, Y.; Aksimentiev, A.; Tajkhorshid, E.; Schulten, K. *Curr. Opin. Struct. Biol.* **2005**, *15*, 423–431.
(4) Wimley, W. C. *Curr. Opin. Struct. Biol.* **2003**, *13*, 404–411.
(5) Borgnia, M.; Nielsen, S.; Engel, A.; Agre, P. *Annu. Rev. Biochem.* **1999**, *68*, 425–458.
(6) Verkman, A. S.; Mitra, A. K. *Am. J. Physiol. Renal Physiol.* **2000**, *278*, F13–F28.
(7) Fujiyoshi, Y.; Mitsuoka, K.; de Groot, B. L.; Philippsen, A.; Grubmuller, H.; Agre, P.; Engel, A. *Curr. Opin. Struct. Biol.* **2002**, *12*, 509–515.
(8) Bichet, D.; Haass, F. A.; Jan, L. Y. *Nat. Rev. Neurosci.* **2003**, *4*, 957–967.
(9) Long, S. B.; Campbell, E. B.; MacKinnon, R. *Science* **2005**, *309*, 897–903.
(10) Long, S. B.; Tao, X.; Campbell, E. B.; MacKinnon, R. *Nature* **2007**, *450*, 376–U3.
(11) Harris, R. A.; Mihic, S. J.; Dildymayfield, J. E.; Machu, T. K. *FASEB J.* **1995**, *9*, 1454–1462.
(12) Gandhi, C. S.; Rees, D. C. *Science* **2008**, *321*, 1166–1167.
(13) Qi, Z.; Sokabe, M.; Donowaki, K.; Ishida, H. *Biophys. J.* **1999**, *76*, 631–641.
(14) Kuhlman, B.; Dantas, G.; Ireton, G. C.; Varani, G.; Stoddard, B. L.; Baker, D. *Science* **2003**, *302*, 1364–1368.
(15) Kaplan, J.; DeGrado, W. F. *Proc. Natl. Acad. Sci. U. S. A.* **2004**, *101*, 11566–11570.
(16) Tsai, C.-J.; Zheng, J.; Nussinov, R. *PLoS Comput Biol* **2006**, *2*, e42.
(17) Jackel, C.; Kast, P.; Hilvert, D. *Annu. Rev. Biophys.* **2008**, *37*, 153–173.
(18) Murakami, Y.; Kikuchi, J.; Hisaeda, Y.; Hayashida, O. *Chem. Rev.* **1996**, *96*, 721–758.
(19) Fiammengo, R.; Crego-Calama, M.; Reinhoudt, D. N. *Curr. Opin. Chem. Biol.* **2001**, *5*, 660–673.
(20) Ghadiri, M. R.; Granja, J. R.; Milligan, R. A.; McRee, D. E.; Khazanovich, N. *Nature* **1993**, *366*, 324–327.
(21) Okamoto, H.; Nakanishi, T.; Nagai, Y.; Kasahara, M.; Takeda, K. *J. Am. Chem. Soc.* **2003**, *125*, 2756–2769.
(22) Baudry, Y.; et al. *Adv. Funct. Mater.* **2006**, *16*, 169–179.
(23) Sanchez-Ouesada, J.; Isler, M. P.; Ghadiri, M. R. *J. Am. Chem. Soc.* **2002**, *124*, 10004–10005.
(24) Boon, J. M.; Smith, B. D. *Curr. Opin. Chem. Biol.* **2002**, *6*, 749–756.
(25) Jordan, E.; Bell, R. G.; Wilmer, D.; Koller, H. *J. Am. Chem. Soc.* **2006**, *128*, 558–567.
(26) Saufi, S. M.; Ismail, A. F. *Carbon* **2004**, *42*, 241–259.
(27) Duke, M. C.; da Costa, J. C. D.; Do, D. D.; Gray, P. G.; Lu, G. Q. *Adv. Funct. Mater.* **2006**, *16*, 1215–1220.
(28) Ghadiri, M. R.; Granja, J. R.; Buehler, L. K. *Nature* **1994**, *369*, 301–304.
(29) Kobuke, Y.; Ueda, K.; Sokabe, M. *J. Am. Chem. Soc.* **1992**, *114*, 7618–7622.
(30) Hummer, G.; Rasaiah, J. C.; Noworyta, J. P. *Nature* **2001**, *414*, 188–190.
(31) Skoulidas, A. I.; Ackerman, D. M.; Johnson, J. K.; Sholl, D. S. *Phys. Rev. Lett.* **2002**, *89*, 185901.
(32) Holt, J. K.; Park, H. G.; Wang, Y. M.; Stadermann, M.; Artyukhin, A. B.; Grigoropoulos, C. P.; Noy, A.; Bakajin, O. *Science* **2006**, *312*, 1034–1037.
(33) Majumder, M.; Chopra, N.; Andrews, R.; Hinds, B. J. *Nature* **2005**, *438*, 44–44.
(34) Wang, Z. K.; Ci, L. J.; Chen, L.; Nayak, S.; Ajayan, P. M.; Koratkar, N. *Nano Lett.* **2007**, *7*, 697–702.
(35) Whitby, M.; Quirke, N. *Nat. Nanotechnol.* **2007**, *2*, 87–94.
(36) Liu, H. M.; Murad, S.; Jameson, C. J. *J. Chem. Phys.* **2006**, *125*, 084713.
(37) Wang, B.; Král, P. *J. Am. Chem. Soc.* **2006**, *128*, 15984–15985.
(38) Král, P.; Shapiro, M. *Phys. Rev. Lett.* **2001**, *86*, 131–134.
(39) Iijima, S.; Yudasaka, M.; Yamada, R.; Bandow, S.; Suenaga, K.; Kokai, F.; Takahashi, K. *Chem. Phys. Lett.* **1999**, *309*, 165–170.
(40) Sint, K.; Wang, B.; Král, P. *J. Am. Chem. Soc.* **2008**, *130*, 16448–16449.
(41) Fornasiero, F.; Park, H. G.; Holt, J. K.; Stadermann, M.; Grigoropoulos, C. P.; Noy, A.; Bakajin, O. *Proc. Natl. Acad. Sci. U. S. A.* **2008**, *105*, 17250–17255.
(42) Liu, B.; Li, X. Y.; Li, B. L.; Xu, B. Q.; Zhao, Y. L. *Nano Lett.* **2009**, *9*, 1386–1394.
(43) Solares, S. D.; Blanco, M.; Goddard, W. A. *Nanotechnology* **2004**, *15*, 1405–1415.
(44) Wan, R.; Li, J.; Lu, H.; Fang, H. *J. Am. Chem. Soc.* **2005**, *127*, 7166–7170.
(45) Li, J. Y.; Gong, X. J.; Lu, H. J.; Li, D.; Fang, H. P.; Zhou, R. H. *Proc. Natl. Acad. Sci. U. S. A.* **2007**, *104*, 3687–3692.
(46) Bianco, A.; Kostarelos, K.; Partidos, C. D.; Prato, M. *Chem. Comm.* **2005**, *5*, 571–577.
(47) Wang, B.; Král, P.; Thanopulos, I. *Nano Lett.* **2006**, *6*, 1918–1921.
(48) Krishnan, A.; Dujardin, E.; Treacy, M. M. J.; Hugdahl, J.; Lynum, S.; Ebbesen, T. W. *Nature* **1997**, *388*, 451–454.
(49) Gilje, S.; Han, S.; Wang, M.; Wang, K. L.; Kaner, R. B. *Nano Lett.* **2007**, *7*, 3394–3398.
(50) Hashimoto, A.; Yorimitsu, H.; Ajima, K.; Suenaga, K.; Isobe, H.; Miyawaki, J.; Yudasaka, M.; Iijima, S.; Nakamura, E. *Proc. Natl. Acad. Sci. U. S. A.* **2004**, *101*, 8527–8530.
(51) Balasubramanian, K.; Burghard, M. *Small* **2005**, *1*, 180–192.
(52) Guo, X.; Whalley, A.; Klare, J. E.; Huang, L.; O'Brien, S.; Steigerwald, M.; Nuckolls, C. *Nano Lett.* **2007**, *7*, 1119–1122.

(53) Kale, L.; Skeel, R.; Bhandarkar, M.; Brunner, R.; Gursoy, A.; Krawetz, N.; Phillips, J.; Shinozaki, A.; Varadarajan, K.; Schulten, K. *J. Comput. Phys.* **1999**, *151*, 283–312.
(54) MacKerell, A. D. *J. Phys. Chem. B* **1998**, *102*, 3586–3616.
(55) Adiga, S. P.; Brenner, D. W. *Nano Lett.* **2005**, *5*, 2509–2514.
(56) Ellis, R. J.; Vandervies, S. M. *Annu. Rev. Biochem.* **1991**, *60*, 321–347.
(57) Wang, B.; Král, P. *Small* **2007**, *3*, 580–584.
(58) Feller, S. E.; Zhang, Y. H.; Pastor, R. W.; Brooks, B. R. *J. Chem. Phys.* **1995**, *103*, 4613–4621.
(59) Cumings, J.; Zettl, A. *Science* **2000**, *289*, 602–604.
(60) Ma, H.; Gruebele, M. *J. Comput. Chem.* **2006**, *27*, 125–134.
(61) Pickett, S. D.; Sternberg, M. J. E. *J. Mol. Biol.* **1993**, *231*, 825–839.
(62) Humphrey, W.; Dalke, A.; Schulten, K. *J. Mol. Graph.* **1996**, *14*, 33–&.
(63) Simonson, T.; Brooks, C. L. *J. Am. Chem. Soc.* **1996**, *118*, 8452–8458.
(64) Fasshauer, D.; Antonin, W.; Subramaniam, V.; Jahn, R. *Nat Struct Mol Biol* **2002**, *9*, 144–151.
(65) Erilov, D.; Puorger, C.; Glockshuber, R. *J. Am. Chem. Soc.* **2007**, *129*, 8938–8939.
(66) Ali, M.; Yameen, B.; Neumann, R.; Ensinger, W.; Knoll, W.; Azzaroni, O. *J. Am. Chem. Soc.* **2008**, *130*, 16351–16357.
(67) Ali, M.; Mafe, S.; Ramirez, P.; Neumann, R.; Ensinger, W. *Langmuir* **2009**, *25*, 11993–11997.

JP9103933